# The Pacific Cold Tongue: A Pathway for Interhemispheric Exchange*

BERNADETTE M. SLOYAN,+ GREGORY C. JOHNSON, AND WILLIAM S. KESSLER

*NOAA/Pacific Marine Environmental Laboratory, Seattle, Washington*

(Manuscript received 29 January 2002, in final form 28 October 2002)

ABSTRACT

Mean meridional upper-ocean temperature, salinity, and zonal velocity sections across the Pacific Ocean between 8°S and 8°N are combined with other oceanographic and air–sea flux data in an inverse model. The tropical Pacific Ocean can be divided into three regions with distinct circulation patterns: western (143°E–170°W), central (170°–125°W), and eastern (125°W–eastern boundary). In the central and eastern Pacific the downward limbs of the shallow tropical cells are $15(\pm 13) \times 10^6$ m$^3$ s$^{-1}$ in the north and $20(\pm 11) \times 10^6$ m$^3$ s$^{-1}$ in the south. The Pacific cold tongue in the eastern region results from diapycnal upwelling through all layers of the Equatorial Undercurrent, which preferentially exhausts the lightest (warmer) layers of the Equatorial Undercurrent [$10(\pm 6) \times 10^6$ m$^3$ s$^{-1}$] between 125° and 95°W, allowing the denser (cooler) layers to upwell [$9(\pm 4) \times 10^6$ m$^3$ s$^{-1}$] east of 95°W and adjacent to the American coast. An interhemispheric exchange of $13(\pm 13) \times 10^6$ m$^3$ s$^{-1}$ between the southern and northern Pacific Ocean forms the Pacific branch of the Pacific–Indian interbasin exchange. Southern Hemisphere water enters the tropical Pacific Ocean via the direct route at the western boundary and via an interior (basin) pathway. However, this water moves irreversibly into the North Pacific by upwelling in the eastern equatorial Pacific and air–sea transformation that drives poleward interior transport across 2°N.

## 1. Introduction

A striking feature of the Pacific Ocean is the equatorial sea surface temperature (SST) minimum that extends from the coast of the Americas into the central Pacific—the cold tongue (Wyrtki 1981). Knauss (1966) suggested that the salinity, temperature, and nutrient distribution in the central and eastern equatorial Pacific Ocean was the result of equatorward convergence into the Equatorial Undercurrent (EUC) and subsequent upwelling. Upwelling in the eastern Pacific Ocean provides a route by which subtropical water can influence the tropical SST, either through property anomalies (Gu and Philander 1997) or transport anomalies (Kleeman et al. 1999). Upwelling also creates the zonal SST gradient that is coupled to the Walker circulation. However, the processes that control the intensity and extent of the mean cold tongue are not well known.

Many observational and modeling studies have analyzed the fate of the EUC. Wyrtki (1981) and Bryden and Brady (1985) constructed large regional box models and found that upwelling from the EUC leads to the equatorial SST minimum. From the heat budget Wyrtki (1981) deduced that the maximum upwelling occurred in the upper EUC, while Bryden and Brady (1985) suggested that the water upwelling to form the cold tongue comes equally from meridional and zonal convergence. One model of the EUC termination in the east has an inertial jet with diapycnal mixing gradually losing volume through upwelling from successively denser layers (Pedlosky 1988), consistent with the observed eastward cooling of the cold tongue. Observational analysis also suggests that the EUC supplies some of the coastal upwelling off South America (Lukas 1986).

In the present study, inverse methods are used to combine a new mean temperature, salinity, and direct velocity climatology (Johnson et al. 2002) with air–sea flux climatologies and historical conductivity–temperature–depth (CTD) and expendable bathythermography (XBT) data in the eastern Pacific to estimate a tropical Pacific circulation that is consistent with the observed data. While the particular focus of the present study is to determine processes that influence the strength of the eastern Pacific cold tongue, the extension of the model domain across the Pacific Ocean also enables investigation of circulation pathways that transport water from the South Pacific to the North Pacific, feeding the Pacific–Indian interbasin exchange. The new climatology, constructed from 172 contemporaneous meridional

* Pacific Marine Environmental Laboratory Contribution Number 2440.

+ Current affiliation: Department of Physical Oceanography, Woods Hole Oceanographic Institution, Woods Hole, Massachusetts.

*Corresponding author address:* Dr. Bernadette Sloyan, Dept. of Physical Oceanography, MS 21, Woods Hole Oceanographic Institution, Woods Hole, MA 02543.
E-mail: bsloyan@whoi.edu

CTD/acoustic Doppler current profiler (ADCP) sections taken across the tropical Pacific, mostly during the 1990s, greatly improves the quality, quantity and spatial coverage of data available compared to that used in earlier volume constraint studies (Wyrtki 1981; Bryden and Brady 1985). A 25-box inverse model was constructed for the tropical Pacific that explicitly includes the diapycnal property transport, meridional eddy heat flux induced by tropical instability waves (TIW) and air–sea transformation driven by horizontal wind-driven mixing and buoyancy fluxes.

This paper is structured as follows. A brief description of the model and data is given in section 2. Initial analyses of the individual model boxes showed that these could be grouped into three broad regions. A detailed description of the circulation of each region is given in section 3. Section 4 draws together the circulation of the three regions and discusses their impact on the Pacific cold tongue. Conclusions are given in section 5.

## 2. Inverse model and data

The geographical domain of the study extends from 8°S to 8°N and from 143°E to the American West Coast. The primary data used are 10 meridional upper-ocean sections of temperature, salinity, and zonal velocity located at 143°E, 156°E, 165°E, 180°, 170°W, 155°W, 140°W, 125°W, 110°W, and 95°W, thus spanning most of the tropical Pacific Ocean. The data and fitting procedures used to construct the mean field studied here are discussed elsewhere (Johnson et al. 2002). Zonal sections constructed at ±2° and ±8° latitude further subdivide the study domain, with additional CTD and XBT data used to determine mean water property distributions and meridional velocity fields at ±8° between 95°W and the American coast.

This combination of meridional and zonal sections divides the tropical Pacific Ocean into 25 boxes (Fig. 3). The inverse model of Sloyan and Rintoul (2000) is developed further and applied to these data to provide an estimate of the circulation of the upper tropical Pacific Ocean that is consistent with the temperature, salinity, velocity, and surface forcing data. The model is forced with surface buoyancy fluxes and wind stress from the Comprehensive Ocean–Atmosphere Data Set (COADS) climatology (da Silva et al. 1994). Eleven potential density surfaces divide the upper 500 m into 11 layers (Table 1). Mass ($M$), temperature ($T$), and salt ($S$) are conserved in all layers. The model system of simultaneous equations is solved by the Gauss–Markov technique (Wunsch 1996). The zonal sections at 8°S and 8°N and 2°S and 2°N divide the northern and southern tropical sectors from the equatorial sectors. The many meridional sections allow exploration of the zonal evolution of the circulation.

While the zonal ($u$) velocities used in the model are directly measured by ADCP to 350–400 m, they are extended to 500 m by melding the ADCP $u$ estimates with geostrophic $u$ below 250 m. This level is conveniently below the core of the EUC. Geostrophic $u$ is calculated from the mean temperature and salinity sections (Johnson et al. 2002) (applying equatorial $\beta$-plane dynamics within ±1° of the equator). The vertical shear of $u$ from the ADCP is small between 275 and 375 m. The reference velocities (at each latitude along each section) are estimated as the mean differences of the ADCP $u$ and geostrophic $u$ over this depth interval. This procedure reproduces both the strong eastward $u$ associated with the EUC and subsurface countercurrents [SCCs: northern (NSCC) and southern (SSCC)] and the westward $u$ of the South Equatorial Current [SEC: northern branch SEC(N) between 4°N to 0° and southern branch SEC(S) between 0° to 8°S] and deeper Equatorial Intermediate Current (EIC; Fig. 1).

The ADCP provides estimates of both $u$ and the meridional ($v$) velocity components. However, in the equatorial region the variability of $v$ is large so the ADCP data provide only a noisy estimate of the small mean $v$ (Johnson et al. 2001). Therefore, we estimate $v$ between the meridional sections assuming geostrophy (referenced to 895 m) and Ekman dynamics. Zonal sections at ±8° and ±2° latitude are formed from the mean temperature and salinity profiles (Johnson et al. 2002). Mean zonal sections between 95°W and the coast of the Americas at 8°S and 8°N are produced from historical CTD and XBT data using similar mapping techniques to those applied by Johnson et al. (2002). These sections extend the model domain from 95°E to the coast, and

TABLE 1. Isopycnal surfaces that define the 11 layers of the inverse model. The 11 layers are grouped into four general water classes, whose average thickness is given.

| Model surface | $\sigma_\theta$ (kg m$^{-3}$) | Model layer | Water class | Thickness (m) |
|---|---|---|---|---|
| | surface | | | |
| 1 | 21.3 | 1 | Surface and mixed layer | 30 |
| | 21.3 | | | |
| 2 | 21.7 | 2 | | |
| | 21.7 | | | |
| 3 | 22.5 | 3 | | |
| | 22.5 | | | |
| 4 | 23.0 | 4 | | |
| | 23.0 | | Upper thermocline water | 120 |
| 5 | 24.0 | 5 | | |
| | 24.0 | | | |
| 6 | 25.5 | 6 | | |
| | 25.5 | | Lower thermocline water | 70 |
| 7 | 26.1 | 7 | | |
| | 26.1 | | | |
| 8 | 26.3 | 8 | | |
| | 26.3 | | Thermostad water | 238 |
| 9 | 26.5 | 9 | | |
| | 26.5 | | | |
| 10 | 26.7 | 10 | | |
| | 26.7 | | | |
| 11 | 26.9 | 11 | | |

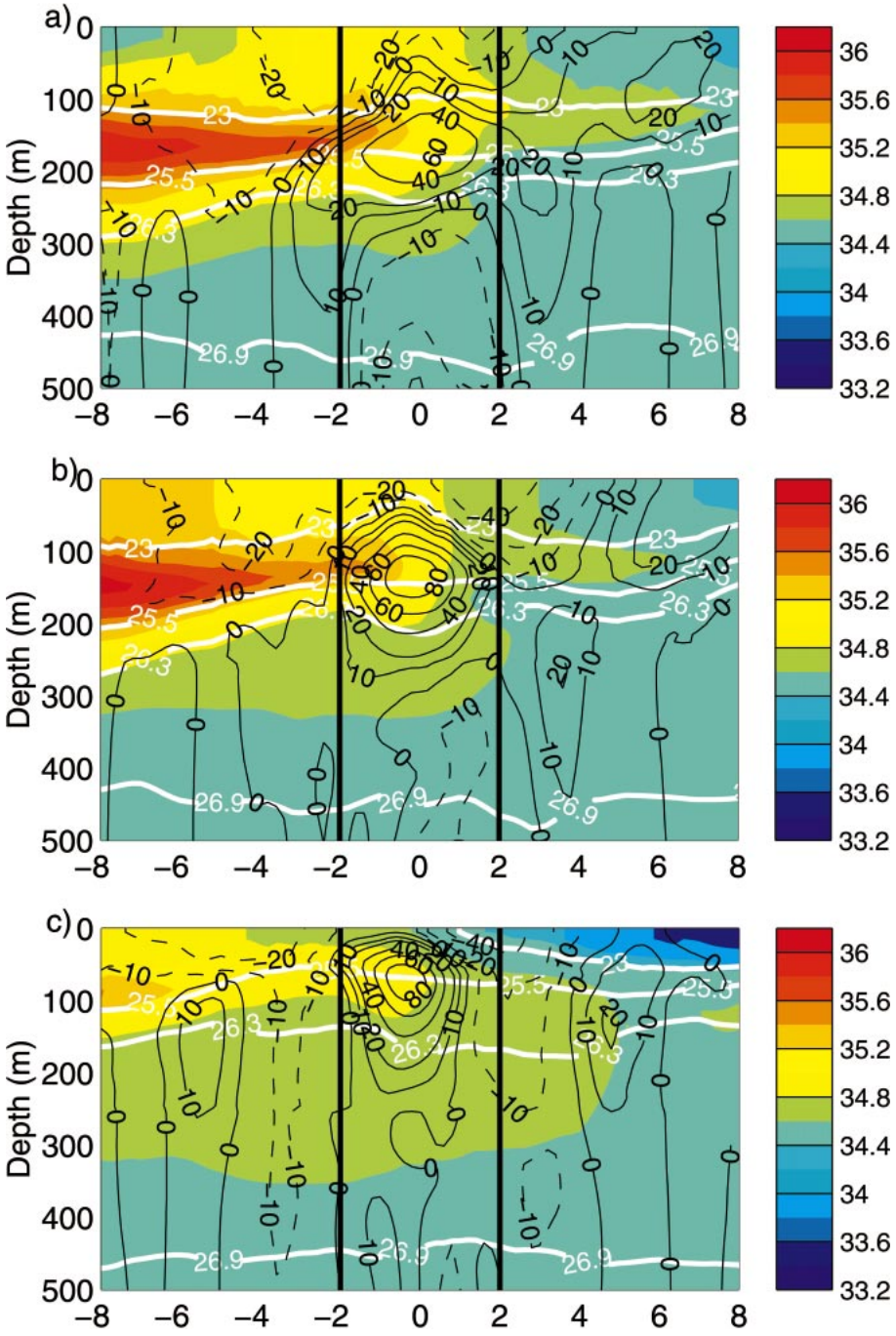


FIG. 1. Salinity (pss-78 shaded) and initial zonal velocity, $u$ (black contours, $10^{-2}$ m s$^{-1}$ solid line eastward, dashed line westward) distribution at (a) 180°, (b) 155°W, and (c) 110°W. Also shown are the four potential density (kg m$^{-3}$) surfaces (white contours) that divide the water column into the four general water classes used in this study.

resolve eastern boundary currents, such as those off Peru.

The construction of zonal sections at ±8° and ±2° latitude distinguish the EUC from the SEC and SCCs and separates the equatorial upwelling and near-equatorial downwelling of the shallow tropical recirculation cells (Lu et al. 1998; Johnson 2001). Previous tropical Pacific volume budget studies (e.g., Wyrtki 1981; Bryden and Brady 1985; Meinen et al. 2001) placed their zonal boundaries at ±5° latitude. This latitude was chosen because midlatitude geostrophy and Ekman dynamics become unreliable for $v$ closer to the equator. Our study

uses the techniques of Lagerloef et al. (1999) to estimate geostrophic and Ekman $v$ at $\pm 2°$ of the equator.

The transition between midlatitude and equatorial dynamics is problematic. Lagerloef et al. (1999) estimated weighting functions such that the geostrophic velocity ($U_g$) is the weighted sum of equatorial and midlatitude formulations:

$$U_g = W_f U_f + W_\beta U_\beta, \tag{1}$$

where $U = u + iv$ and the subscripts $g$, $f$, and $\beta$ represent the (merged) geostrophic velocity, midlatitude ($f$ plane) geostrophy, and equatorial ($\beta$ plane) geostrophy, respectively. Lagerloef et al. (1999) prescribed the weight functions $W_f$ and $W_\beta$ to vary inversely with the meridional structure of the respective error variance of $U_f$ and $U_\beta$, such that the minimum variance is given to the weighted sum of (1). Using surface drifter data, they found that the weight functions can be approximated at a given latitude ($\theta$) by a Gaussian function with the meridional decay scale ($\theta_s$) a free parameter,

$$W_\beta = \exp\left[-\left(\frac{\theta}{\theta_s}\right)^2\right], \qquad W_f = 1 - W_\beta. \tag{2}$$

The best fit of $\theta_s$ to drifter data was 2.2°. This length scale is comparable to the first baroclinic mode Rossby radius near the equator, 200–250 km (Gill 1982; Chelton et al. 1998). Scaling the transition from midlatitude to equatorial dynamics by the equatorial Rossby radius also has some theoretical support. Moore and Philander (1977) applied a steady wind to an unbounded equatorial ocean that was initially at rest. Their solution showed a transition from zonal acceleration on the equator to a steady Ekman response off the equator that scaled by the equatorial radius of deformation.

Thus, following Lagerloef et al. (1999) the weighted sum of the midlatitude and equatorial geostrophic $v$ at $\pm 2°$ latitude provided an initial estimate of the mean geostrophic $v$ across these zonal sections. The same weighting functions were applied to the Ekman transport at $\pm 2°$. Mean $v$ produced by this method was found to be small in comparison to $u$, generally $<5$ cm s$^{-1}$ (Fig. 2).

The inverse model conservation equation illustrates the balance among advection, diapycnal transport, and surface forcing. For a layer bounded by interface $m$ and $m + 1$,

$$\sum_{j=1}^{N}\left[\Delta x_j \int_{h_m}^{h_{m+1}} \rho c_j (U + b)_j \, dz\right] + (E_j c_j)_{\text{meridional}} + (w_c Ac)_m - (w_c Ac)_{m+1} + (F_c + F_c^*)_m - (F_c + F_c^*)_{m+1} = 0. \tag{3}$$

Here $\Delta x_j$ is the station spacing at pair $j$ and $c_j$ is the property value per unit mass at this pair. The initial estimate of the velocity $U$ is determined from the CTD, ADCP, and XBT data; $E_j c_j$ is the meridional Ekman property transport at pair $j$; $w_c Ac$ is the property diapycnal transport across isopycnal layer $m$ beneath the sea surface, including mechanical mixing in the mixed layer where isopycnals are nearly vertical; and $F_c$ is the total transformation driven by horizontal wind mixing and surface buoyancy forcing across an outcropping isopycnal. The subsequent system of simultaneous equations is solved for the unknown velocity adjustments $b_j$, the diapycnal property transfer rate $w_c$ (with $c = M$, $T$, $S$) for the $m$th interface, and corrections to the wind-driven horizontal mixing and air–sea climatologies $F_c^*$.

In the central and eastern equatorial Pacific (155°–95°W) mixing across the SST fronts bounding the cold tongue, induced by TIWs, results in a net heat convergence into the equatorial Pacific (Hansen and Paul 1984; Baturin and Niiler 1997; Kessler et al. 1998). These studies suggest that the magnitude of meridional eddy heat flux (100–180 W m$^{-2}$) is larger than the air–sea heat flux. Hansen and Paul (1984) found that the northern TIWs dominate the eddy heat flux term and suggested an eddy heat flux ratio of 0.75 to 0.25 between the northern and southern TIWs, respectively. In our study we added an additional constraint to the temperature conservation equations to include the effects of the TIW eddy heat flux. In the upper 60 m between 155° and 95°W, heat equivalent to a surface heat flux of 100 W m$^{-2}$ between 2°S and 2°N was transferred into the equatorial sector from the northern (75%) and southern (25%) sectors.

The solutions determined by inverse methods are greatly influenced by uncertainties in the initial estimates of the velocity, diapycnal transfer rate and air–sea fluxes (solution variance), and conservation statements (model variance). A priori layer conservation variances of (3 Sv)$^2$ for mass, (2 Sv $\times$ layer mean temperature)$^2$ for temperature, and (5 Sv $\times$ layer mean salt)$^2$ for salt are assumed (Sv $\equiv 10^6$ m$^3$ s$^{-1}$). An additional constraint was that the entire region should balance to within an a priori variance of (4 Sv)$^2$. No other constraints (e.g., Indonesian throughflow transport or heat flux) were imposed on the model.

The errors in absolute $u$ from the ADCP include instrumental and navigational error, data processing errors, mapping errors, and probably most significantly, geophysical aliasing errors from sparse temporal sampling. Considering these potential sources of error, we assume an a priori variance for $u$ of $(6 \times 10^{-2}$ m s$^{-1})^2$. At $\pm 8°$, $v$ is the sum of geostrophic and Ekman estimates and we assign a variance of $(1 \times 10^{-2}$ m s$^{-1})^2$. However, the more involved $v$ estimates at $\pm 2°$ (see

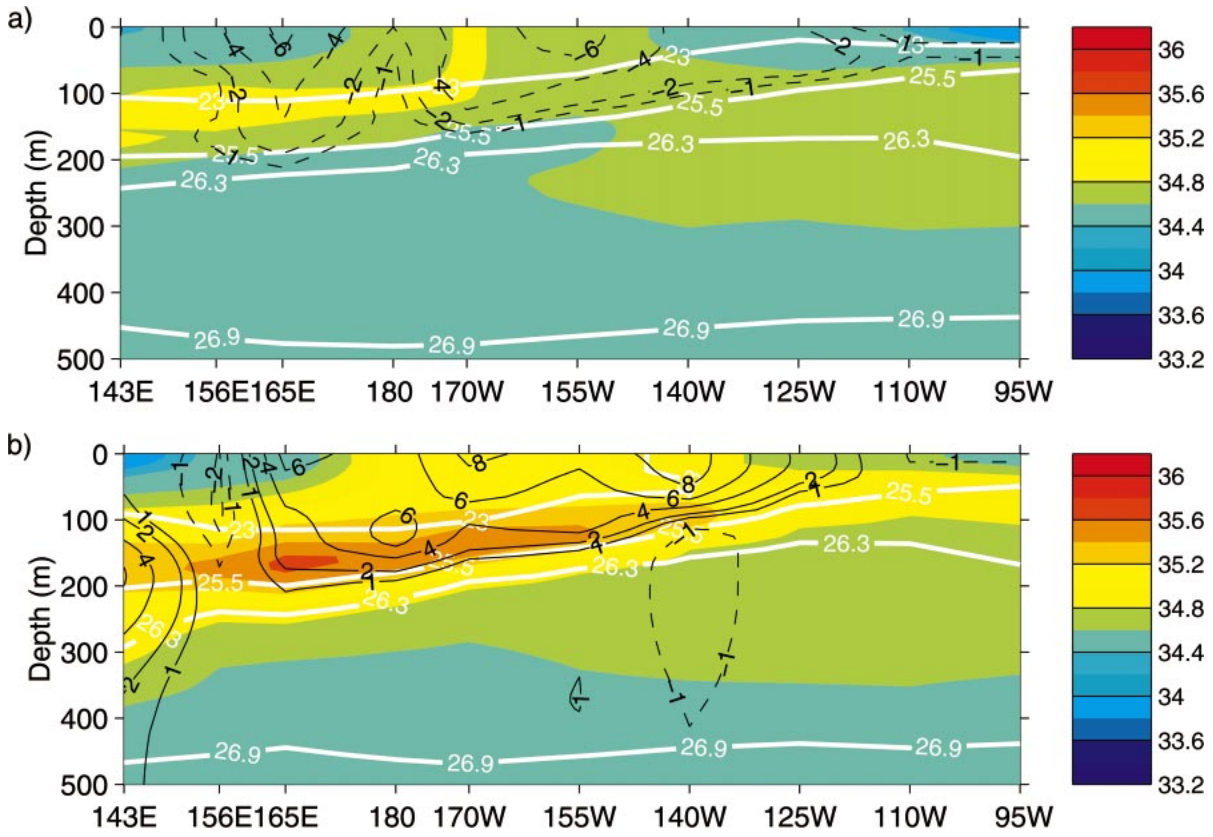


FIG. 2. Salinity (pss-78 shaded) and initial meridional geostrophic velocity $v$ (black contours, $10^{-2}$ m s$^{-1}$ solid line northward, dashed line southward) distribution at (a) 2°N, and (b) 2°S. Also shown are the four potential density (kg m$^{-3}$) surfaces (white contours) that divide the water column into the four general water classes used in this study.

above) require a higher a priori variance, and we chose the value $(3 \times 10^{-2}$ m s$^{-1})^2$.

Previous studies have found significant vertical and cross-isothermal ($\approx$ diapycnal) mixing in the tropical Pacific Ocean (e.g., Wyrtki 1981; Bryden and Brady 1985; Johnson et al. 2001; Meinen et al. 2001) and also indicate a strong depth dependence to the vertical velocity. Given the expected depth dependency of diapycnal mixing, we assumed an a priori variance of $(2 \times 10^{-5}$ m s$^{-1})^2$ for the upper nine isopycnal surfaces ($\sigma_\theta \leq 26.5$ kg m$^{-3}$) and $(2 \times 10^{-6}$ m s$^{-1})^2$ for remaining isopycnal layers ($26.7 \leq \sigma_\theta \leq 26.9$ kg m$^{-3}$).

Finally, the errors associated with any air–sea flux climatology are thought to be large (Speer and Tziperman 1992; Barnier et al. 1995; Josey et al. 1999). However, error estimates for the climatologies are rarely provided. In this study we assumed an a priori variance which is a factor of (2 $\times$ magnitude of wind stress and freshwater flux)$^2$ and (50 W m$^{-2}$)$^2$ for the heat flux.

As stated, a priori model and solution variances greatly influence the model solution and associated errors. We have attempted to quantify these variances to the best of our ability and in all cases have tried not to underestimate these variances. As a result, the posterior errors are likely to represent upper bounds on uncertainties of the tropical Pacific Ocean circulation determined by the model. Model solutions run with reasonable perturbations to the a priori variances are the same, within the given error, as those presented here.

## 3. Regional circulation

The zonal evolution of the tropical Pacific currents implied by the inversion (Table 2 and Fig. 3) can be compared with previous estimates from a variety of studies, methods and longitudes (Table 3). The estimated current transports from this study and previous studies, at corresponding longitudes, are similar apart from the North Equatorial Countercurrent (NECC) where the present study definition of the NECC as eastward transport between 4° and 8°N for $\sigma_\theta \leq 25.5$ is more restrictive than that used in previous studies (Gouriou and Toole 1993; Johnson et al. 2002). The study boundary at 8°N results in an incomplete sampling of the NECC, particularly in the eastern Pacific. Also the SEC(S) extends to 15°–20°S (Church and Boland 1983) but the present sampling only extends to 8°S. Johnson et al. (2002) present a detailed description of the mean zonal currents and water properties, their seasonal cycle, and ENSO cycle.

TABLE 2. Transport estimates ($\times 10^6$ m$^3$ s$^{-1}$) for the tropical Pacific currents. The zonal currents are defined as SEC westward transport between 8°S and 4°N for $\sigma_\theta \leq 26.3$ kg m$^{-3}$; EIC deep westward transport lying beneath the EUC; SCCs eastward transport poleward of ±2° for $\sigma_\theta \geq 25.5$ kg m$^{-3}$ and/or eastward transport between the equator and ±2° for $\sigma_\theta \geq 26.3$ kg m$^{-3}$; EUC eastward transport within ±2° of the equator for $22.5 \leq \sigma_\theta \leq 26.3$ kg m$^{-3}$, although east of and including 110°W the density range extends to $\sigma_\theta \leq 26.7$ kg m$^{-3}$; NECC eastward transport north of approximately 4°N for $\sigma_\theta \leq 25.50$ kg m$^{-3}$. New Guinea Coastal Undercurrent (NGCU) westward transport adjacent to the southern boundary for $24.0 \leq \sigma_\theta \leq 26.9$ kg m$^{-3}$. Errors quoted represent the formal error of the inverse method, i.e., the error associated with determining velocity adjustments. Asterisks indicate current not found at section.

| Current | 143°E | 156°E | 165°E | 180° | 170°W | 155°W | 140°W | 125°W | 110°W | 95°W |
|---|---|---|---|---|---|---|---|---|---|---|
| SEC (S) | −9.3 ± 1.0 | −2.0 ± 1.5 | −15.1 ± 2.0 | −23.6 ± 1.7 | −20.7 ± 1.9 | −19.0 ± 2.1 | −19.1 ± 2.1 | −13.5 ± 1.1 | −14.3 ± 1.8 | −6.2 ± 2.5 |
| SEC (N) | * | −0.5 ± 0.6 | −0.3 ± 0.4 | −2.0 ± 0.5 | −6.9 ± 0.8 | −12.6 ± 1.0 | −22.0 ± 1.8 | −13.3 ± 2.3 | −15.9 ± 2.1 | −11.2 ± 2.3 |
| EIC | −0.8 ± 0.5 | −2.8 ± 1.0 | −7.4 ± 0.9 | −7.9 ± 1.1 | −3.2 ± 1.0 | −4.0 ± 1.2 | −1.0 ± 0.6 | −0.1 ± 1.6 | −0.8 ± 0.6 | −0.3 ± 0.4 |
| SSCC | * | 9.6 ± 1.3 | 6.7 ± 2.2 | 8.3 ± 2.0 | 9.0 ± 1.5 | 6.7 ± 1.8 | 6.4 ± 1.9 | 6.6 ± 2.2 | 6.1 ± 1.9 | 3.8 ± 2.4 |
| EUC | 8.2 ± 0.8 | 19.8 ± 0.8 | 18.2 ± 1.1 | 23.0 ± 1.1 | 24.2 ± 0.8 | 26.4 ± 1.9 | 25.3 ± 1.4 | 30.5 ± 2.0 | 24.0 ± 1.9 | 16.2 ± 1.9 |
| NSCC | * | 11.5 ± 1.5 | 7.6 ± 1.7 | 6.7 ± 1.8 | 10.9 ± 1.8 | 7.6 ± 2.0 | 4.5 ± 2.0 | 5.5 ± 1.8 | 6.4 ± 2.2 | 5.7 ± 2.4 |
| NECC | * | 17.1 ± 1.4 | 13.1 ± 1.3 | 13.9 ± 1.2 | 9.1 ± 1.0 | 10.4 ± 0.8 | 11.4 ± 0.9 | 6.0 ± 0.7 | 2.1 ± 0.5 | 5.3 ± 0.4 |
| NGCU | −14.7 ± 1.5 | * | * | * | * | * | * | * | * | * |

TABLE 3. Transport estimates ($\times 10^6$ m$^3$ s$^{-1}$) for the tropical Pacific currents from previous studies at a variety of locations. D&H: Delcroix and Héin (1988), SURTROPAC direct measurement from free-falling current profiler at 165°E; DEH: Delcroix et al. (1987), SURTROPAC CTD data at 165°E semiannual between 1984 and 1986, referenced to 1000 m and free-falling direct velocity measurements; G&T: Gouriou and Toole (1993), combination of SURTROPAC, US/PRC and TEW spanning 1984 to 1991 for western Pacific; K&T: Kessler and Taft (1987), pre-El Niño mean between 180° and 150°W using XBT data and a mean temperature–salinity relation for the central Pacific, relative to 450 m and poleward of ±2° of equator; L&F: Lukas and Firing (1984), from Hawaii-to-Tahiti Shuttle Experiment, direct velocity measurements from profiling current mooring and CTD data referenced to 400 dbar, respectively; W&K: Wyrtki and Kilonsky (1984), CTD sections of the Hawaii-to-Tahiti Shuttle Experiment (central Pacific) referenced to 1000 m; Leetmaa (1982), direct observations, eastern Pacific between 2°S and 1°N to a lower temperature of 13.5°C; HTM: Hayes et al. (1983), EPOCS data at 110°W between 1979 and 1981, referenced to 500 dbar; P&T: Picaut and Tournier (1991), Pacific Ocean XBT data from 1979 to 1985, poleward of ±2° of equator. Asterisks indicate current estimate not given or current not found at particular sections.

| | Western | | | | | Central | | | Eastern | | All regions |
|---|---|---|---|---|---|---|---|---|---|---|---|
| Current | D&H 165°E | DEH 165°E | | G&T 165°E | | K&T 180°–150°W | L&F ≈155°W | W&K ≈155°W | Leetmaa 110° and 95°W | HTM 110°W | P&T W,C, and E |
| SEC (S) | * | * | | * | | −35.1 ± 5.1 | * | −29.3 | * | * | * |
| SEC (N) | * | −38.8 ± 17.5 | | * | | * | * | −11.0 | * | * | * |
| Total SEC | * | * | −24.8 | −37.7 | −41.7 | * | * | −40.3 | * | * | 33.2 ± 7.0 |
| EIC | −7.0 ± 4.8 | * | −4.5 | −4.9 | −2.6 | * | * | −9.8 | * | * | * |
| SSCC | * | 8.8 ± 2.6 | 7.6 | 6.5 | 10.6 | * | * | 4.3 | * | * | * |
| EUC | * | 19.7 ± 7.3 | 15.3 | 17.3 | 26.1 | * | 32.2 ± 3.5 | 25.6 ± 17 30.3 | 20.2 8.0 | * | * |
| NSCC | * | 14.8 ± 7.0 | 11.7 | 11.4 | 11.1 | * | * | 7.7 | * | 13.7 ± 1.6 | * |
| NECC | * | 27.4 ± 13.5 | 20.4 | 19.6 | 18.9 | 21.1 ± 5.7 | * | 19.2 | * | 8.3 ± 2.8 | 17.8 ± 8.0 |

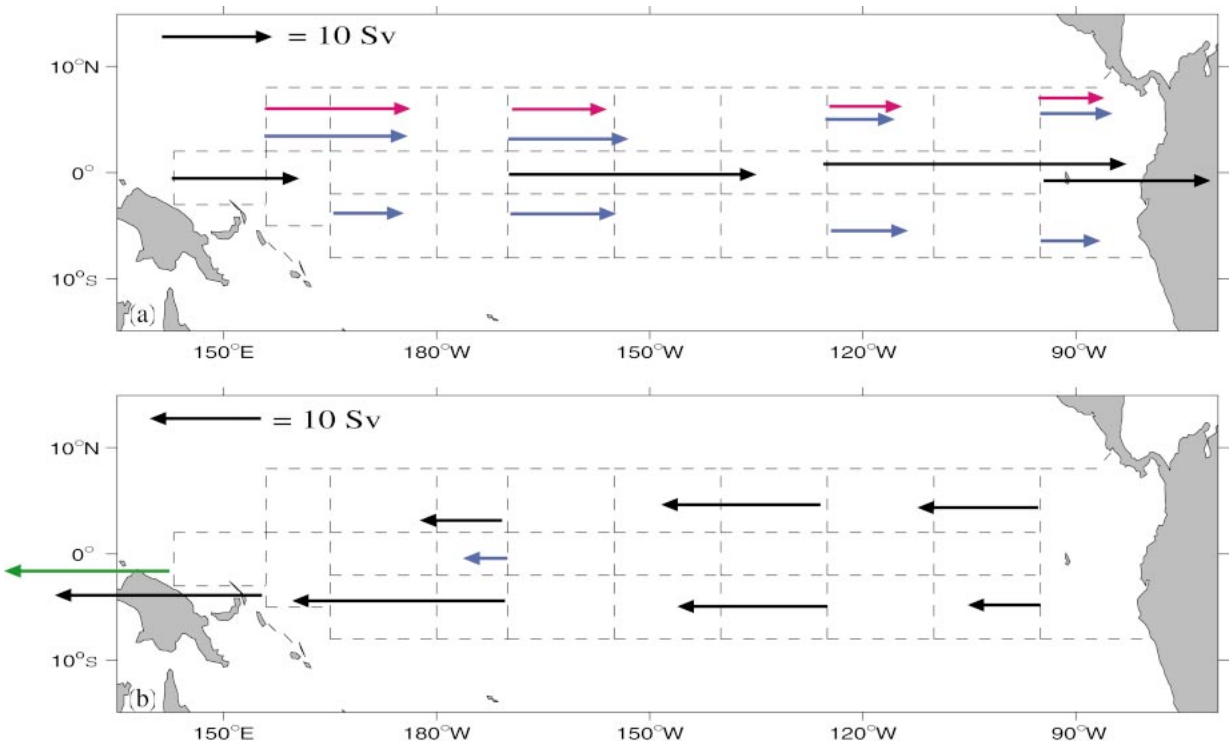


FIG. 3. Volume transport ($\times 10^6$ m$^3$ s$^{-1}$) of tropical Pacific currents. (a) Eastward currents: EUC (black), SCCs (blue), and NECC (pink). (b) Westward currents: SEC(S,N) (black) and EIC (blue). The westward component of the NGCU (green) is also shown. Transports are only given at the boundaries separating the western and central region (170°W), central and eastern region (125°W), and at extreme western (143° and 156°E) and eastern (95°W) sections. Also shown are the box (25) regions (dashed lines) used in the inverse model. The boundaries are formed from a combination of CTD and ADCP data (Johnson et al. 2002) and historical CTD and XBT data in the eastern Pacific.

The individual 25 boxes of the tropical Pacific can be grouped into three large regions with distinct circulation patterns: the western region from the 143°E to 170°W, the central region between 170° and 125°W, and the eastern region from 125°W to the coast of the Americas. The 11 isopycnals describe four general water classes (Table 1). Important features of the tropical Pacific circulation are described for each region, water class, and sector (southern 8°–2°S, equatorial 2°S–2°N, and northern 2°–8°N). Henceforth, we will describe transports between these boxes, which combine eastward and westward currents. For example, boxes from 2° to 8°N include both the eastward NECC and part of the westward SEC.

### *a. Western region*

The western region circulation is complicated by the termination of the SEC and EIC; the development of the EUC, SCCs, and NECC; and connections among these currents with the low-latitude western boundary currents: the New Guinea Coastal Current (NGCC), New Guinea Coastal Undercurrent (NGCU), New Ireland Coastal Undercurrent (NICU), and Mindanao Current (MC; Tsuchiya et al. 1989; Butt and Lindstrom 1994). An additional complication in the model is that the southern boundary of the western Pacific region steps around the coast of New Guinea with sections at 8°, 5°, and 3°S (Fig. 3). For simplicity these steps are combined and shown schematically as transport at 8°S (Fig. 4 and Table 4).

The outer islands of the Bismarck Archipelago (New Ireland and Bougainville Islands) and New Guinea form the western boundary of the equatorial Pacific Ocean. The SEC impinging on this region is north of its bifurcation zone at ~15°S (Church and Boland 1983) and feeds the salty equatorward NGCU and NICU (Tsuchiya et al. 1989; Butt and Lindstrom 1994). Observational and model studies (Pedlosky 1987; Tsuchiya et al. 1989; Pedlosky 1991; Butt and Lindstrom 1994) suggest that the high salinity NGCU and NICU feed the EUC. Tsuchiya et al. (1989) asked whether the NGCU overshoots the equator to then retroflect and flow eastward with the EUC, similar to observations (Flagg et al. 1986) of the North Brazil Current in the Atlantic Ocean, and as suggested by theories of equatorial western boundary dynamics (Anderson and Moore 1979). CFC property distributions support such a hypothesis, with a South Pacific CFC minimum extending north to 2°N (Fine et al. 1994).

In our model we find westward transport of the NGCC and NGCU at 143°E and significant eastward transport at 156°E north of 2°N (Table 4) with a salinity signature

similar to that of the NGCU, consistent with the property and theoretical studies mentioned above. In the equatorial sector, at 143°E, the eastward transport of the lower thermocline ($25.5 \leq \sigma_\theta \leq 26.3$ kg m$^{-3}$) EUC and westward component of the NGCU effectively balance (Fig. 4 and Table 4).

The inverse solution suggests that the NGCU does, in fact, overshoot the equator and retroflect back to feed the EUC between 156°E and 170°W. This plus equatorward flow of upper and lower thermocline water across 2° and 3°S are major contributors to the increased transport of the EUC in the western Pacific. The remaining contribution comes from the North Pacific, identified by fresher water within the EUC.

Tsuchiya (1991) also found northwest thermostad transport in the NGCU. He suggested that the thermostad SCCs originate from surface and thermocline water of the Tasman Sea, although both southern and northern properties are found in the NSCC (Gouriou and Toole 1993; Bingham and Lukas 1995; Johnson and McPhaden 1999). Our study shows a complex set of interconnections among the equatorward western boundary currents (MC, NGCU, and NICU), the westward EIC, and the eastward SCCs.

In this study the SCCs, found within the thermostad ($26.3 \leq \sigma_\theta \leq 26.9$ kg m$^{-3}$), attain near-constant eastward transport by 165°E, although a local maximum is found at 170°W (Table 2). Transport of the westward EIC, found beneath the EUC and flanked by the SCCs, reaches a maximum between 170°W and 180°. The SCCs eastward transport, at 170°W, is greater than that of the westward EIC in the equatorial sector and results in a net eastward thermostad property transport in all sectors (Fig. 4 and Table 4). The property transport across the southern boundary is poleward between 165°E and 170°W (8°S), but farther west between 143° and 165°E (at 3° and 5°S) net property transport in the thermostad layer of the NGCU/NICU is equatorward.

Much of the NGCU flows unmodified through the southwest corner of the model domain and leaves at the western boundary (143°W). Eastward and equatorward thermostad property transports are found at the zonal and meridional boundaries of the northern sector. The retroflection of the NGCU results in equatorward transport across 2°N (165°E–170°W) that feeds both the increased westward transport of the EIC and the NSCC. The EIC terminates before reaching the western boundary by poleward transport across 2°S that, together with the NGCU/NICU, ultimately feeds the SSCC. Equatorward transport across 8°N feeds North Pacific thermostad water into the NSCC. In the western region the inversion suggests that isopycnal mixing within the thermostad dominates and diapycnal mixing is not significant.

### *b. Central region*

In the central Pacific (170°–125°W), unlike the western region, the classical 3D tropical circulation (Cromwell 1953; Knauss 1966; Wyrtki and Kilonsky 1984; Lu et al. 1998) is seen. The zonal currents (EUC, SEC, NECC, and SCCs) are fully developed and the thermocline shoals to the east. Equatorial upwelling and surface poleward transport (Fig. 5 and Table 4) form the upward and surface limbs of the shallow tropical and subtropical cells (Lu et al. 1998). Off-equatorial downwelling and subsurface meridional equatorward transport complete the shallow tropical cells. Within the thermostad a complicated interaction among the deep currents occurs, and Southern Hemisphere water feeds the extension of the EUC into the thermostad.

Lu et al. (1998) document the indirect observational and model evidence for the existence of the shallow tropical circulation cell. Recent observational analysis suggests that half of the water upwelling at the equator downwells within ±8° of the equator (Johnson 2001), but does not quantify the subsurface limbs. The present study provides further direct observational evidence for the shallow tropical cells (Fig. 5 and Table 4). The northern and southern tropical cells exhibit poleward surface transport, diapycnal downwelling (Figs. 6a,c) between ±2° and ±8° of 8(±5) and 10(±9) Sv, respectively, equatorward upper thermocline transport across ±2°, and closing equatorial upwelling. The equatorward upper thermocline transport across ±2° effectively balances the large equatorial diapycnal upwelling of 24(±4) Sv of upper thermocline water to the surface/mixed layer.

The conversion of 24(±4) Sv of EUC upper thermocline water to surface/mixed layer (Fig. 6b, right panel) results from the combined action of wind-driven horizontal mixing, air–sea heat fluxes, and equatorward TIW eddy heat fluxes as the EUC shoals along its eastward path. Vertical mixing associated with the upward slope of the isopycnals (Fig. 6, left panel) does not result in the transformation of water between the upper thermocline and surface/mixed layer water classes. Between 155° and 125°W the assumed TIW eddy heat flux (100 W m$^{-2}$), distributed in the upper 60 m, adds heat to the surface/mixed layer and shoaling upper thermocline. The TIW heat flux to the upper thermocline layer results in an interior diapycnal heat flux of 4 W m$^{-2}$ from the upper thermocline to the surface/mixed layer. The inversion correction to the air–sea heat flux increases the initial COADS heat flux from 64 to 81 W m$^{-2}$ (155°–125°W). These heat fluxes to the surface/mixed layer feed the 204 W m$^{-2}$ net advective (poleward and zonal)

→

FIG. 4. Circulation of the western Pacific region for (a) volume ($\times 10^6$ m$^3$ s$^{-1}$), (b) temperature (PW), and (c) salt ($\times 10^6$ kg s$^{-1}$) transports. Ekman transport is included in the meridional transport estimates. Lateral and zonal transports are solid arrows. Lateral transports at 2°S and 2°N are shown (red arrows) on back face. Diapycnal property transport between layer interfaces for the southern, equator, and northern regimes are shown on front face. Water classes are separated by bounding isopycnal surfaces-surface/mixed layer (red),

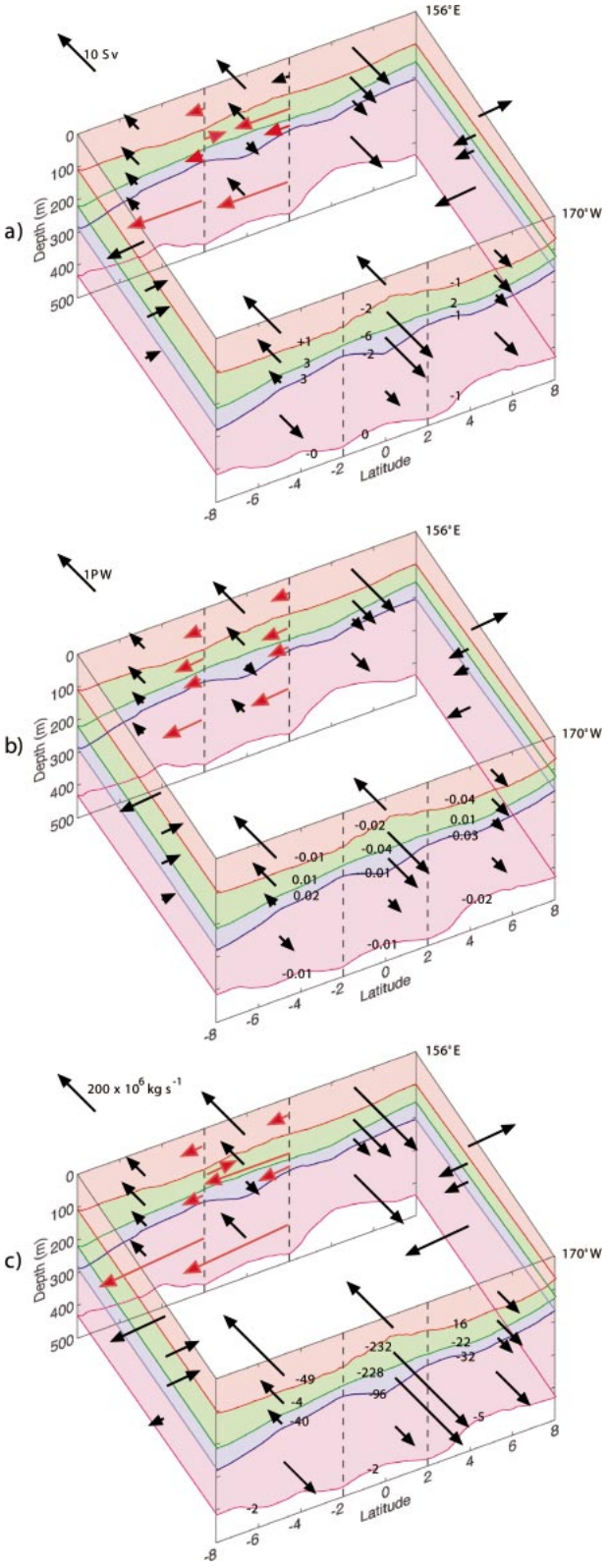


FIG. 4. (*Continued*) upper thermocline (green), lower thermocline (blue), and thermostad (pink). Note that although the boundary of the southern sector is shown at 8°S for simplicity, it is actually found over a range of latitudes in the western region.

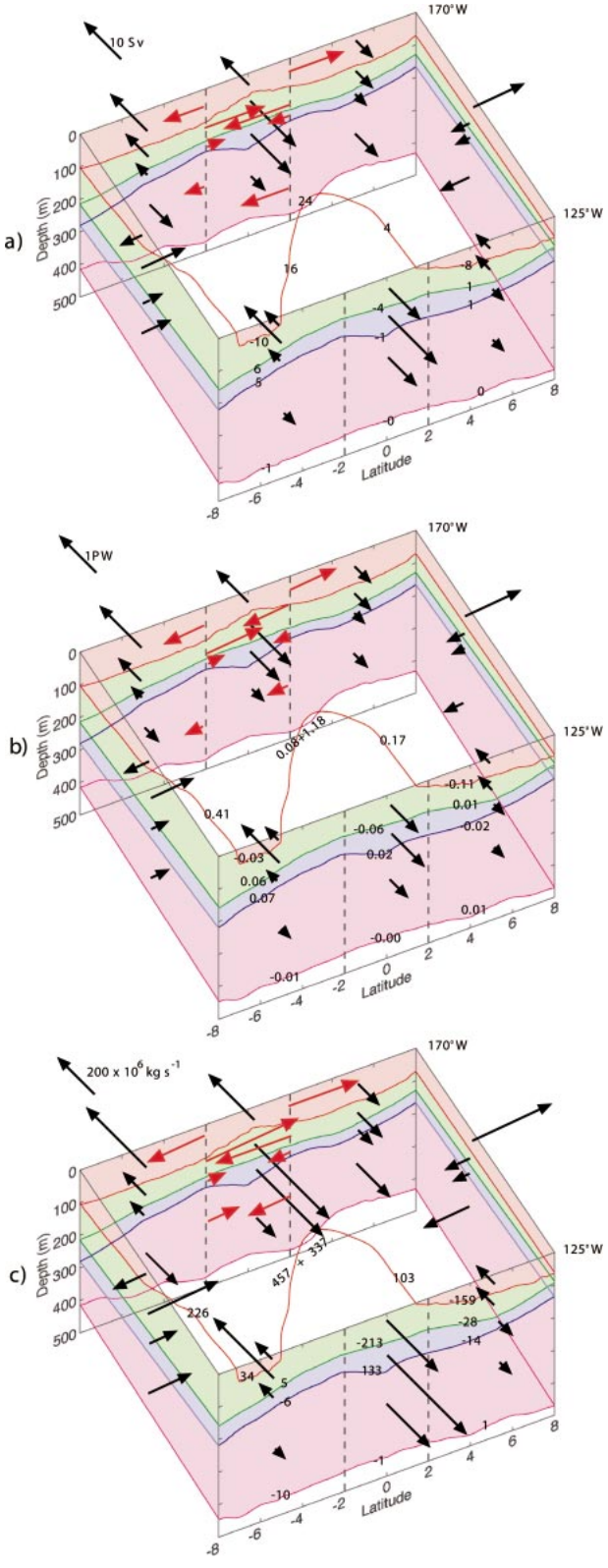


FIG. 5. As in Fig. 4 but for central Pacific region. Air–sea transformations are shown at outcropping isopycnal. In the equatorial sector, interior diapycnal transports, where significant, are also shown at the outcropping isopycnal.

TABLE 4. (a) Total meridional transport (including Ekman) extimates ($\times 10^6$ m$^3$ s$^{-1}$) for the western, cental, and eastern Pacific regions at 8°S, 2°S, 2°N, and 8°N and (b) net zonal transport at the boundaries separating the western and central region (170°W), central and eastern region (125°W), and at the extreme western (southern 165°E, equator 143°E, and northern 156°E) and eastern (95°W) sections for southern, equator, and northern sectors. Transport estimates are given for each water class: S/ML, surface and mixed layer; UTW, upper thermocline water; LTW, lower thermocline water; and TW, thermostad water. Positive is northward or eastward. Note that in the western Pacific region while the meridional transport of the southern boundary is nominally given at 8°S for simplicity, it actually steps around the coast of New Guinea with sections at 8°S, 5°S, and 3°S. Also in the eastern Pacific region the 2°S and 2°N boundary does not exterd to the America; transport estimates are between 125° and 95°W. Asterisks indicate water class not found at section. Transport estimates are shown graphically in Figs. 4, 5, and 7.

(a)

| | Western | | | | Central | | | | Eastern | | | |
|---|---|---|---|---|---|---|---|---|---|---|---|---|
| Water class | 8°S | 2°S | 2°N | 8°N | 8°S | 2°S | 2°N | 8°N | 8°S | 2°S | 2°N | 8°N |
| S/ML | −6.2 ± 2.4 | −0.7 ± 1.4 | −0.1 ± 1.8 | 6.5 ± 1.6 | −3.8 ± 1.1 | −6.4 ± 0.9 | 11. 8 ± 1.0 | 11.6 ± 1.0 | * | * | 6.2 ± 0.4 | 2.9 ± 0.8 |
| UTW | 4.0 ± 2.2 | 1.8 ± 0.8 | −9.6 ± 1.4 | −2.3 ± 0.8 | 8.0 ± 1.2 | 12.6 ± 1.3 | −14.5 ± 1.1 | −1.6 ± 0.7 | 1.8 ± 1.6 | −6.6 ± 0.9 | −1.8 ± 0.9 | 1.3 ± 0.4 |
| LTW | 3.8 ± 1.4 | −0.9 ± 0.4 | −2.5 ± 0.6 | −1.5 ± 0.6 | 2.1 ± 0.9 | 1.0 ± 0.7 | −1.4 ± 0.7 | −0.4 ± 0.7 | 1.7 ± 1.2 | 1.3 ± 1.5 | 3.5 ± 1.7 | 3.2 ± 1.2 |
| TW | 0.7 ± 4.5 | −15.0 ± 3.8 | −12.7 ± 4.1 | −6.5 ± 4.2 | 3.8 ± 4.6 | −0.8 ± 3.3 | −7.5 ± 4.3 | −1.4 ± 4.7 | 4.5 ± 4.7 | 10.2 ± 4.8 | 8.1 ± 4.9 | 8.4 ± 4.0 |

(b)

| | 143°–165°E | | | 170°W | | | 125°W | | | 95°W | | |
|---|---|---|---|---|---|---|---|---|---|---|---|---|
| Water class | Southern | Equator | Northern | Southern | Equator | Northern | Southern | Equator | Northern | Southern | Equator | Northern |
| S/ML | −1.9 ± 0.8 | −7.1 ± 0.7 | 10.3 ± 0.7 | −10.0 ± 0.7 | −7.3 ± 0.5 | 2.6 ± 0.6 | −1.6 ± 0.1 | −0.4 ± 0.1 | −1.6 ± 0.4 | * | −1.2 ± 0.1 | 1.2 ± 0.3 |
| UTW | −2.8 ± 0.6 | −3.3 ± 0.6 | 5.6 ± 0.5 | −5.0 ± 0.5 | 12.9 ± 0.4 | 3.2 ± 0.4 | −10.1 ± 0.7 | 8.4 ± 0.5 | −1.8 ± 0.4 | −3.6 ± 0.4 | 1.3 ± 0.3 | 0.1 ± 0.2 |
| LTW | −1.1 ± 0.3 | 0.6 ± 0.4 | 1.5 ± 0.3 | −1.0 ± 0.3 | 11.4 ± 0.3 | 1.2 ± 0.2 | −1.1 ± 0.4 | 14.0 ± 0.4 | 1.2 ± 0.4 | 0.2 ± 0.6 | 9.9 ± 0.7 | 1.0 ± 0.7 |
| TW | −1.3 ± 1.4 | −3.8 ± 1.4 | 7.8 ± 1.4 | 4.6 ± 1.4 | 2.0 ± 1.4 | 5.0 ± 1.6 | 0.2 ± 1.9 | 7.0 ± 1.6 | 0.6 ± 2.0 | 0.8 ± 1.9 | 1.7 ± 1.4 | 1.3 ± 1.8 |

heat divergence. These terms balance to within the overall formal uncertainty of 23 W m$^{-2}$.

Equatorial upwelling estimates for the central Pacific are often provided in depth coordinates which combine both diapycnal upwelling and the eastward shoaling of isopycnals (e.g., Wyrtki 1981; Poulain 1993; Weisberg and Qiao 2000; Johnson et al. 2001). In general, these studies find upwelling from the EUC to the surface/mixed layer. The Weisberg and Qiao (2000) and Johnson et al. (2001) vertical velocity profiles showed strongest upwelling across the EUC upper thermocline with decreasing but still positive vertical velocity through the EUC lower thermocline. Weisberg and Qiao (2000) also found evidence of downwelling into the thermostad. Bryden and Brady (1985) estimated a velocity of $1 \times 10^{-5}$ m s$^{-1}$ across the 23°C isotherm between 150° and 110°W and smaller downwelling into the thermostad. While their transport estimates were made between 5°S and 5°N, cross-isotherm velocities were calculated assuming confinement to within ±83 km of the equator. The estimated mean cross-isothermal velocity of Meinen et al. (2001) has a similar vertical profile to that of Bryden and Brady (1985), but with significantly reduced magnitude because their estimate (also between ±5°) was not artificially confined to an equatorial strip.

In the present study the equivalent diapycnal velocity needed to convert upper thermocline to surface/mixed layer water (Fig. 6b, left panel) is comparable to that of Bryden and Brady. However, the inversion shows that the net diapycnal mass transport between the surface/mixed layer and upper thermocline is dominated by the effects of wind-driven horizontal mixing across outcropping isopycnals, with the eddy heat fluxes induced by the TIWs adding the necessary additional buoyancy required to convert upper thermocline water to surface/mixed layer water (Fig. 5).

In the equatorial sector of the central region the transport of the EUC increases slightly from west to east (Table 2), although significant upwelling of EUC upper thermocline water is also seen. The increased transport of the EUC is the result of increased transport in the lower thermocline and extension of the EUC to the thermostad layer. Increased transport of the lower thermocline layer is driven by diapycnal downwelling from the EUC upper thermocline and equatorward convergence across ±2° (Fig. 5, Fig. 6b, and Table 4).

In the southern sector poleward transport of surface/mixed layer water across 2°S feeds the increased westward property transport from 125° to 170°W, and together with the air–sea transformation (wind-driven horizontal mixing, and heat and freshwater fluxes) of upper thermocline water to the surface/mixed layer, maintains poleward transport across 8°S (Fig. 5). The small net upward diapycnal temperature and salt transports from the upper thermocline to the surface/mixed layer (Fig. 5) result from a slightly larger upward diffusion from the relatively warm, salty upper thermocline layer that enters the tropical Pacific region across 8°S. The upward

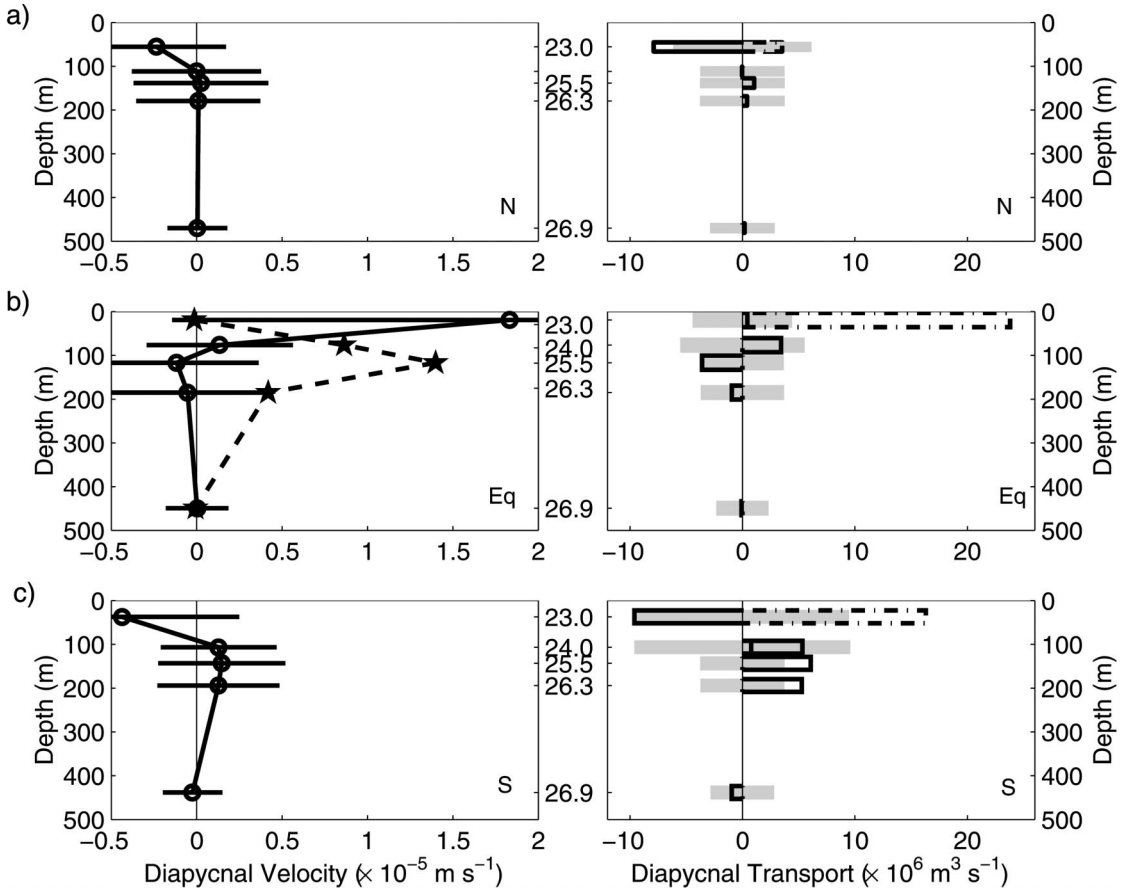


FIG. 6. Diapycnal velocity ($10^{-5}$ m $s^{-1}$, left panel solid line) and transport ($10^6$ $m^3$ $s^{-1}$, right panel solid line) for each sector of the central Pacific: (a) northern, (b) equatorial, and (c) southern. Diapycnal velocities and transports are given for $\sigma_\theta$ = 23.0, 24.0, 25.5, 26.3, and 26.9 kg $m^{-3}$, shown on common (internal) *y* axis. Also shown for the equatorial sector is the along isopycnal ''upwelling'' velocity (dashed). Air–sea diapycnal transports (right panel, dot-dashed) are shown at the outcropping isopycnals. Inverse method errors associated with determining adjustments to the diapycnal transport are shaded (right panel).

diapycnal salt transport is related to the chimneylike structure of salinity in the central Pacific (Johnson et al. 2002). In the northern sector, as in the southern sector, poleward transport in the surface/mixed layer across 8°N is maintained by air–sea transformation (wind-driven horizontal mixing and buoyancy) of upper thermocline water to the surface/mixed layer and net zonal convergence between 125° and 170°W (Fig. 5).

Johnson and McPhaden (1999) and Rowe et al. (2000) describe the property homogeneity equatorward of the SCC cores and the sharp potential vorticity fronts at the SCC cores that delineate the equatorward thermostad water from the poleward components of the SCCs. In the present study, a complex circulation in the thermostad layer is found, with strong horizontal shears among the deep SEC(N,S), SCCs, EUC, and EIC (see Fig. 1c). Thermostad property homogeneity is found to result from mixing between the SCCs equatorward of their core and the deep SEC(N,S). Deep SEC(S,N) water replaces SCC water lost to the equator, while equatorward thermostad transport across ±8° maintains the potential vorticity and property gradients at the SCC cores.

The SCCs diverge poleward as they flow east, and westward flowing deep SEC water wedges between the SCCs and EUC thermostad extension. At 170°W the eastward SCCs dominate (Fig. 5). In the southern and northern sector at 125°W the eastward SCCs and westward deep SEC balance, resulting in small net eastward transports. Isopycnal mixing between the NSCC and deep SEC(N) results in a net equatorward transport of thermostad water across 2°N. Approximately one-half of the SSCC transported eastward in the equatorial sector, at 170°W, moves poleward across 2°S between 170° and 125°W. The SSCC water that remains in the equatorial sector and the equatorward transport across 2°N contributes to both the increased westward transport of the EIC and the extension of the EUC into the thermostad (Fig. 5 and Table 4). Mixing between the poleward trending SSCC and the SEC(S) reduces the westward transport of the SEC(S), homogenizes the ther-

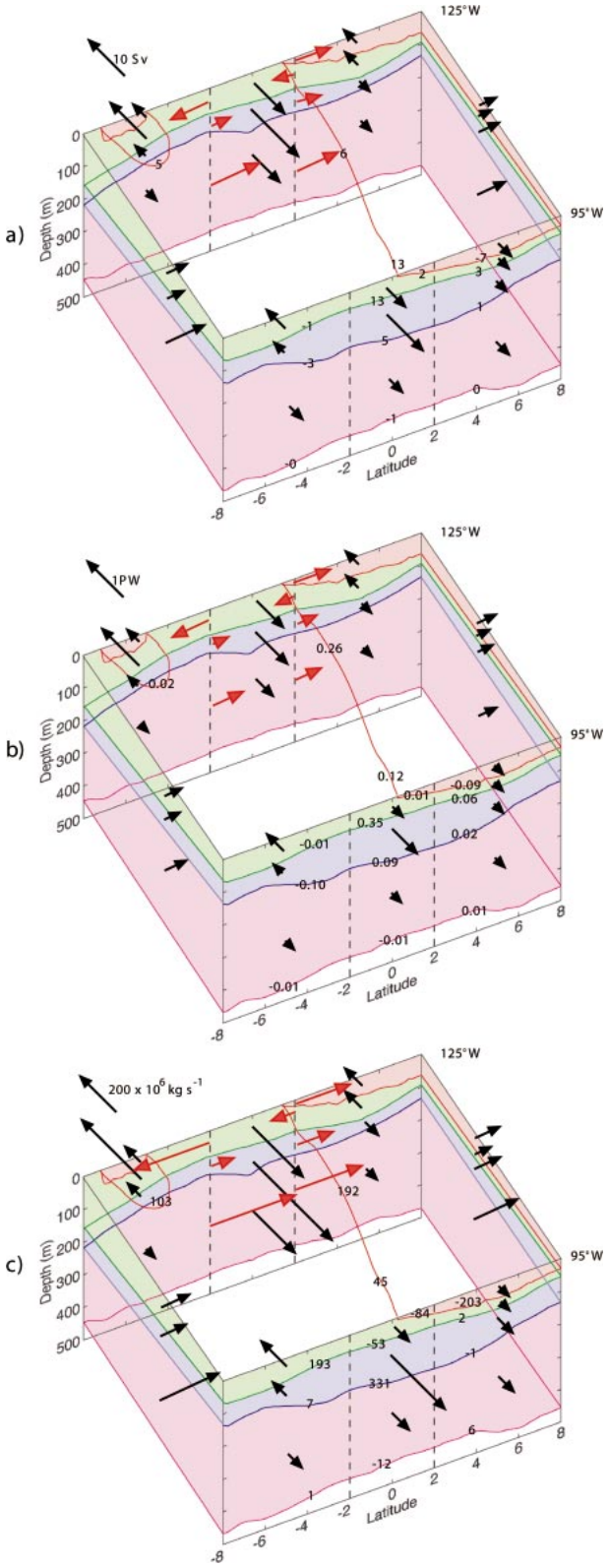


FIG. 7. As in Fig. 4, but for eastern Pacific region. Air–sea transformation are shown at the outcropping isopycnal. At the eastern boundary historical CTD and XBT data close the ±8° sections to the American coast; those transports are combined with transport estimates between 125° and 95°W at ±8°. Sections at ±2° are between 125° and 95°W. Whereas zonal transports at 95°W are shown at the eastern boundary, including those in the equatorial sector, the diapycnal property transports for the region between 95°W and the Americas are folded into the equatorial region.

mostad property gradients equatorward of the SSCC core, and allows diapycnal upwelling of thermostad water to the lower thermocline. Equatorward thermostad transport at ±8°, into the northern and southern sectors, feeds recently ventilated subpolar mode/intermediate water into the tropical Pacific.

### c. Eastern region

In the eastern region the EUC continues to shoal to 110°W (e.g., Johnson et al. 2001). Farther east it shifts southward and terminates (Lukas 1986). Poleward surface transport, off-equator downwelling and subsurface equatorward transport identify the shallow tropical cells (Fig. 7 and Table 4). Equatorial upwelling that exhausts the lightest layers of the EUC, exposing an increasingly denser, colder EUC to the east, results in the eastward cooling of the cold tongue. Lower thermocline and thermostad water that upwell to form the cold tongue are exported into the Northern Hemisphere. As the SCCs approach the eastern boundary, they diverge poleward (Johnson and McPhaden 1999; Kessler 2002) and northern and southern branches of the SEC develop with deep extensions to the thermostad layer. Interior equatorward transport of lower thermocline and thermostad water imports Southern Hemisphere mode water into the tropical region.

In the model the northern and southern boundaries at ±8° are extended from 95°W to the coast of the Americas (Fig. 3). For simplicity the meridional transports across these sections are combined with the meridional transport across ±8° between 125° and 95°W and shown schematically between these longitudes (Fig. 7). While zonal transports at 95°W are shown, the diapycnal property transports for the region between 95°W and the Americas (from 8°S to 8°N) are folded into the equatorial sector (Fig. 7 and Fig. 8b).

The shallow tropical overturning cell is found in the northern and southern sectors—poleward surface transport (surface/mixed layer in the northern region and upper thermocline in the southern sector), downwelling [northern 7(±12) Sv, and southern 10(±7) Sv], and equatorward subsurface transport (Fig. 7, Table 4, Figs. 8a,c). In the southern sector the downward limb of the shallow tropical cell is found across $\sigma_\theta = 24.0$ kg m$^{-3}$, which is within the upper thermocline layer (and thus not shown in Fig. 7, see Fig. 8c). However, the subsurface equatorward convergence does not completely balance the surface poleward divergence. Instead, upwelling from all layers of the EUC feeds the poleward transport (Fig. 8b).

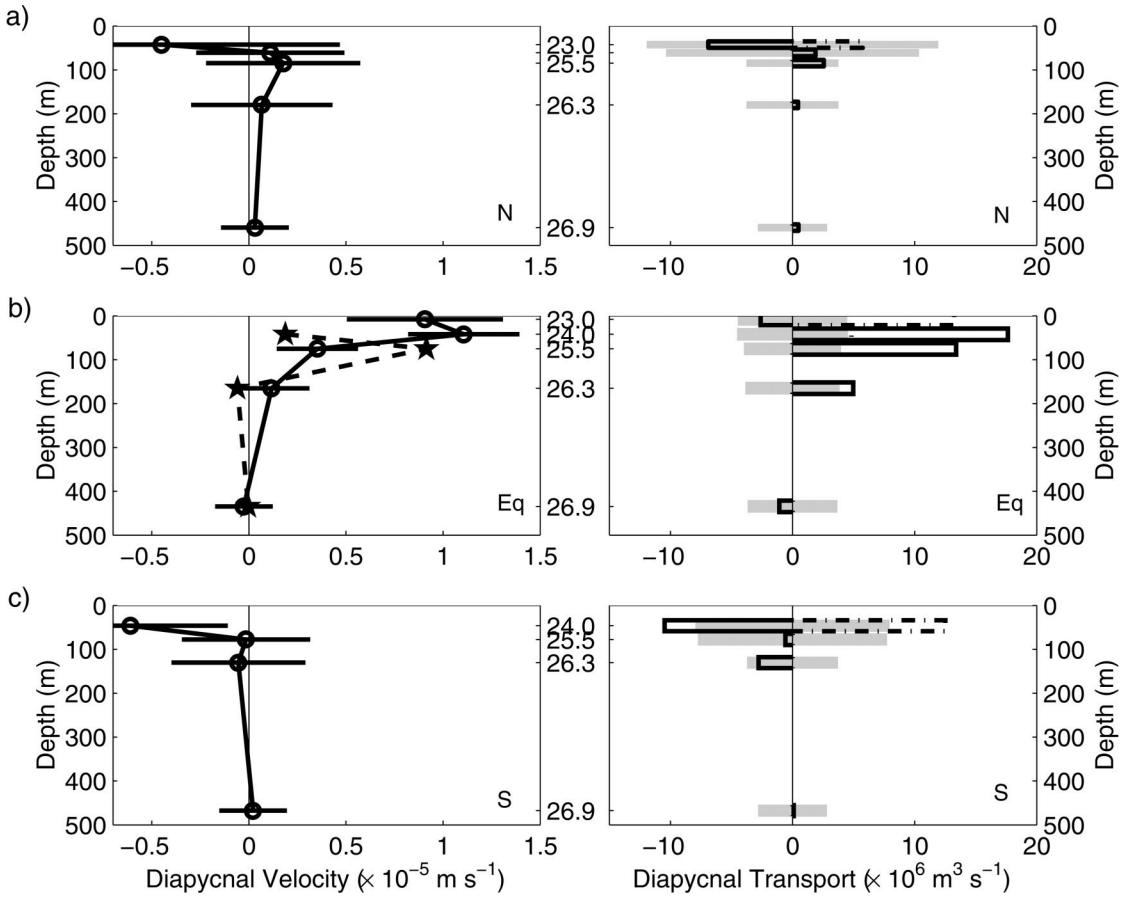


FIG. 8. As in Fig. 6, but for eastern Pacific sectors. Diapycnal velocity and transport for the region between 95°W and the American coast are folded into the equatorial region.

Observational (Lukas 1986) and model (Pedlosky 1987, 1988) studies describe the termination of the EUC. Lukas (1986) suggests that the EUC terminates via upwelling east of the Galapagos Islands between the equator and 5°S. Pedlosky (1988) suggests that the EUC, modeled as an inertial jet in which cross-isopycnal mixing is included, is exhausted before reaching the eastern boundary by gradual upwelling from successively denser EUC layers. The present study suggests that both mechanisms are active in the termination of the EUC.

In the equatorial sector at 125°W, the EUC brings upper and lower thermocline and thermostad water into the region that, together with diapycnal upwelling of mass from all layers of the EUC (Fig. 7 and Fig. 8b), feeds the net poleward transport at 2°S and air–sea transformation of 13($\pm$4) Sv of EUC upper thermocline water to the surface/mixed layer. The upwelling halves the transport of the EUC between 125° and 95°W and the lightest layers of the EUC are exhausted, preferentially exposing an increasingly denser, colder EUC to the east. Much of the diapycnal upwelling (70%) of EUC lower thermocline water occurs in the coastal region between 95°W and the American coast. Between 125° and 95°W the TIW eddy heat flux (100 W m$^{-2}$) and direct air–sea COADS heat flux of 83 W m$^{-2}$, essentially unchanged by the inversion and the 24 W m$^{-2}$ diapycnal heat flux, feed the 184 W m$^{-2}$ net advective (poleward) heat divergence. These terms balance to within the overall formal uncertainty of 44 W m$^{-2}$.

In the southern sector poleward upper thermocline transport at 2°S, westward transport at 95°W and equatorward transport at 8°S, which mark the beginnings of the SEC in the model domain, feed the increased westward transport of the SEC(S) from 95° to 125°W as well as air–sea transformation of upper thermocline water to the surface/mixed layer (Fig. 7 and Table 4). Interior diapycnal downwelling (mass and temperature) from the upper thermocline to the lower thermocline layer is seen, while diapycnal upwelling of salt results in a salt chimney similar to, although weaker than, that seen in the central region (Fig. 7).

Johnson and McPhaden (1999) suggest that the poleward spreading SCCs form the eastward limb of elongated cyclonic gyres, while Rowe et al. (2000) also find anticyclonic gyres. In the present study we find poleward transport across 8°N supporting a cyclonic recirculation, while deep westward transport in the SEC(N,S) in the eastern Pacific support the existence of the an-

ticyclonic gyres (Table 2). However, we find that the southern cyclonic and anticyclonic gyres are not completely closed recirculations.

Thermostad water in the southern sector is transported equatorward at 8° and 2°S (Fig. 7 and Table 4), principally between 125° and 110°W. In the equatorial sector the Southern Hemisphere input and eastward transport of EUC thermostad water at 125°W feed the poleward flow at 2°N and the diapycnal upwelling of EUC thermostad water to EUC lower thermocline water. Further poleward transport of thermostad water across 8°N occurs between 125°W and the Americas where the NSCC turns north under the Costa Rica Dome (Johnson and McPhaden 1999; Kessler 2002).

Equatorward thermostad water transport across the southern boundary feeds Southern Ocean mode/intermediate water into the tropical Pacific. This water follows a convoluted circulation path and eventually supplies equatorward thermostad transport at 2°S. Once within the equatorial region this water may directly upwell into the lower thermocline feeding the equatorial upwelling or circulate within the northern equatorial anticyclonic cell.

## 4. Circulation of the tropical Pacific Ocean and impacts on the cold tongue

The inverse model shows that the circulation of the tropical Pacific can naturally be separated into three regions. West of 170°W the SEC feeds the Southern Hemisphere low-latitude western boundary currents (NGCU, NICU). These equatorward boundary currents are essential elements in the development of the EUC and, together with the EIC, in the development of the SCCs. We find that the NGCU crosses the equator in the far west and retroflects to the equator across 2°N between 143° and 165°E. This, together with direct input from the NICU (2°S) results in the eastward salinity increase of the EUC (Gouriou and Toole 1993). Net equatorward transport across the southern boundary results from these large western boundary transports west of 165°E, partly compensated by poleward (Ekman) transport east of 165°E. This is the signature of the SEC shifting poleward as it approaches the western boundary where mixing in the Solomon and Bismark Seas partly erodes the high salinity SEC signature. These waters form the western boundary currents that eventually feed the EUC.

In the central and eastern regions the downward limbs of the shallow tropical overturning cell are 15(±13) Sv in the north and 20(±11) Sv in the south. The tropical cells are closed by subsurface equatorward transport, equatorial upwelling, and poleward surface transport across ±2°. The lower limbs of the shallow tropical cells feed relatively high and low salinity southern and northern subtropical water, respectively, into the equatorial region that reinforces the sharp salinity front at the equator. In the southern sector the equatorward transport of salinity maximum subtropical mode water increases the transport of the shallow overturning lower limb. This source of Southern Hemisphere water forms part of a net interhemispheric exchange.

Eastward shoaling of the thermocline coupled with diapycnal upwelling from the EUC thermostad through the upper thermocline layers, in the eastern region, results in the equatorial sea surface temperature minimum, the (Pacific) cold tongue. The spatial structure of the cold tongue—eastward cooling of sea surface temperature—is determined by diapycnal upwelling that preferentially exhausts the lightest layers of the EUC along its eastward transit of the eastern region, allowing deeper, colder, EUC lower thermocline and thermostad water to upwell east of 95°W and adjacent to the coast of the Americas. Thus the EUC terminates both through interior upwelling (Pedlosky 1988) of 10(±6) Sv of upper thermocline water and upwelling adjacent to the Americas (Lukas 1986) of 9(±4) Sv of lower thermocline and thermostad water. The buoyancy (heat) input needed to drive the upwelling from the EUC layers is 0.10 PW and 0.13 PW, respectively. Air–sea transformation of 13(±4) Sv of the upwelling EUC water to the surface/mixed layer and poleward transport across 2° and 8°N between 95°W and the American coast allow an interhemispheric transport to occur in the eastern Pacific.

From this study, differences in the strength and depth of equatorial upwelling between the central and eastern region are notable (Fig. 6b and Fig. 8b). (Recall that in the eastern region diapycnal velocity and transports between 95°W and the American coast and 8°N and 8°S are folded into the equatorial upwelling. This may result in an underestimate of the equatorial diapycnal velocity, but not transport, in the eastern Pacific.) In the central region diapycnal upwelling is found above the core of the EUC ($\sigma_\theta \leq 24.0$ kg m$^{-3}$, ~75 m) and weak diapycnal downwelling below the EUC core ($\sigma_\theta \geq 25.5$ kg m$^{-3}$). Air–sea transformation across outcropping isopycnals ($\sigma_\theta \leq 23.0$ kg m$^{-3}$), principally through wind-driven horizontal mixing, is significantly larger than the interior diapycnal transport. However, the heat flux required to support the air–sea transformation is nearly equally derived from the inversion corrected COADS heat flux of 81 W m$^{-2}$ between 155° and 125°W and the imposed 100 W m$^{-2}$ TIW eddy heat flux. In the eastern region diapycnal upwelling extends from the thermostad to the surface/mixed layer ($\sigma_\theta \leq 26.3$ kg m$^{-3}$, ~175 m). In this region interior diapycnal mixing dominates and air–sea transformations play a minor role, apart from in the northern sector.

Bryden and Brady (1985), in the central Pacific, found similar cross-isotherm (≈diapycnal) upwelling velocities above the core of the EUC and smaller upwelling below the core. The differences in diapycnal velocity estimates below the EUC core between the current study and the Bryden and Brady (1985) study is likely a result of the previous study estimating the upwelling rate over an area that combined the central and eastern Pacific

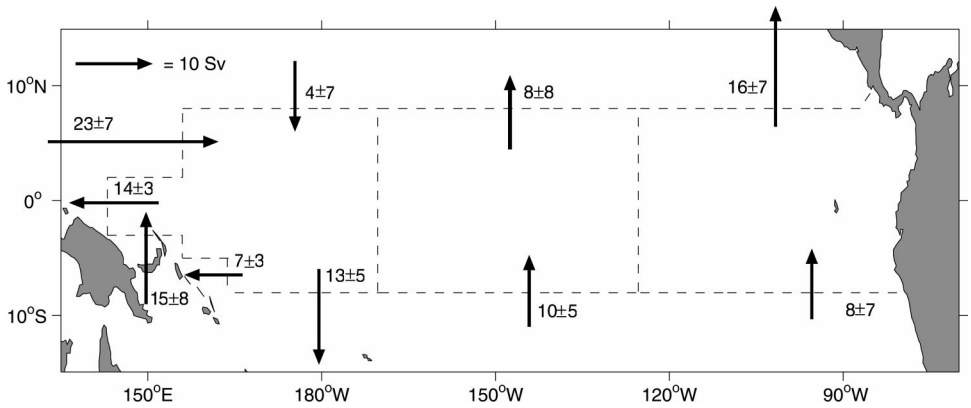


FIG. 9. Net volume transport ($\times 10^6$ m$^3$ s$^{-1}$) across the northern, western, and southern boundaries. The mean $\sigma_\theta$ of meridional transport across the southern boundary is $\sigma_\theta = 24.0$ kg m$^{-3}$ at the western boundary, $\sigma_\theta = 25.5$ kg m$^{-3}$ for the central region, and $\sigma_\theta = 26.7$ kg m$^{-3}$ for the eastern region. Across the northern boundary (8°N) the mean $\sigma_\theta$ density of the equatorward and poleward transport is $\sigma_\theta = 26.3$ kg m$^{-3}$ for the western region, $\sigma_\theta = 22.5$ kg m$^{-3}$ for the central region, and $\sigma_\theta = 25.5$ kg m$^{-3}$ for the eastern region.

regions. The reader is also reminded that while the previous study transport estimates were made between ±5° of the equator, the cross-isothermal velocities were calculated assuming confinement to a narrow equatorial strip.

Net equatorward transport of 13(±13) Sv of Southern Hemisphere water (Fig. 9) forms the Pacific branch of the Pacific–Indian interbasin exchange (Macdonald 1998; Gordon et al. 1999; Sloyan and Rintoul 2001). At the southern boundary of the central region, the transport occurs in the upper thermocline layers (salinity maximum), while at that of the eastern region it occurs in the thermostad layer. In the southern sector of the western region, poleward and westward transport between 165°E and 170°W, principally surface/mixed layer and upper thermocline water, feeds the equatorward low-latitude western boundary currents. The Southern Hemisphere water participates in the tropical Pacific Ocean circulation. The result, in the northern sector, is enhanced eastward transport in all layers in the western region and net northward transport in the surface/mixed layer in the eastern region.

Input of southern origin upper thermocline water in the central Pacific defines the interior (basin) pathway by which South Pacific subtropical water enters the tropical Pacific region (Johnson and McPhaden 1999). The upper thermocline water increases the westward SEC(S) transport and strengthens the lower limb of the Southern Hemisphere shallow tropical overturning cell. Thus, equatorward transport in the southern sector of the central region can feed both direct equatorward interior transport and indirect transport through the equatorward low-latitude western boundary. Thermostad water, whose origin is mode/intermediate water of the Southern Ocean, enters the tropical Pacific in the eastern region and at the western boundary, circulates in and mixes with the SCCs, EIC and deep SEC(N,S). Equatorial upwelling of thermostad water in the eastern Pacific results in the Pacific cold tongue and provides a mechanism by which Southern Hemisphere mode/intermediate water can influence the equatorial Pacific sea surface temperature. The properties of these waters, including their potential vorticity, are reset by surface forcing in the equatorial region and thus can be transported poleward across 2°N in the basin interior. The upwelling in the eastern Pacific is one route by which Southern Ocean mode/intermediate water, participating in the Indian–Pacific interbasin exchange, irreversibly crosses the equator.

## 5. Conclusions

Mean meridional temperature, salinity, and zonal velocity sections (Johnson et al. 2002) and historical CTD and XBT data were combined with COADS surface climatologies by inverse methods to estimate the three-dimensional circulation of the tropical Pacific Ocean. The inversion showed that the circulation of the tropical Pacific Ocean can be divided into three regions: western (143°E to 170°W), central (170°W–125°W), and eastern (125°W–eastern boundary). In the western region mixing between terminating westward currents (SEC and EIC) and low-latitude western boundary currents determines the properties of the eastward EUC, SCCs, and NECC. These interactions occur within similar density horizons and diapycnal property transports are not significant.

The shallow tropical cells [15(±13) Sv in the northern sector and 20(±11) Sv in the southern sector] are seen in the central and eastern regions. In the central region equatorial upwelling of 24(±4) Sv from above the core of the EUC defines the upper limb of the combined shallow tropical and subtropical cells. Decreased poleward transport between ±2° and ±8° and diapycnal downwelling from the surface/mixed layer to the upper thermocline form the poleward and downward limb of

the shallow tropical cell. In the central region the tropical cells are closed by subsurface equatorward transport of upper thermocline water that nearly balances the equatorial upwelling. In spite of this upwelling, EUC transport increases due to equatorward input of lower thermocline and thermostad water, part of the subtropical cells. Similar to this study, modeling studies (e.g., Lu and McCreary 1995; Blanke and Raynaud 1997) found that the shallow tropical overturning cells do not reduce the net transport of the EUC.

The large errors on the meridional and diapycnal transports reflect the upper bounds on uncertainties of these components of the tropical Pacific circulation. The ADCP velocities result in zonal current transports that are well determined. Improving the initial estimate of meridional transport via direct velocity and shear observations will greatly reduce the uncertainties of the meridional and diapycnal mass and property transports.

The Pacific cold tongue in the eastern region results from isopycnal shoaling and from diapycnal upwelling through all layers of the EUC. The spatial structure of the cold tongue—sea surface temperature cooling in an eastward direction—is due to the preferential diapycnal upwelling of lightest (warmer) EUC upper thermocline near 125°W. Upwelling of 10($\pm$6) Sv to the east exhausts the lightest EUC water, exposing cooler, denser EUC water as it approaches the Americas. Adjacent to the coast of the Americas 9($\pm$4) Sv of EUC lower thermocline and thermostad water upwells, resulting in the coolest sea surface temperature.

A net 13($\pm$13) Sv transport from the southern to the northern Pacific Ocean is implied by the inversion. The net equatorward transport across the southern boundary is achieved at the western boundary via western boundary currents (NGCU and NICU), via interior transport of upper thermocline salinity maximum water in the central region and via equatorward transport of thermostad water in the eastern region. Southern Hemisphere water that enters the tropical Pacific Ocean moves into the North Pacific by upwelling in the eastern equatorial Pacific and air–sea transformation which drives the poleward transport across 2° and 8°N between 95°W and the Americas. In particular, Southern Ocean thermostad (mode/intermediate) water that enters the tropical Pacific participates in the circulation of and mixing between the SCCs, EIC, and deep SEC(N,S), eventually feeding the dense thermostad water that upwells in the eastern Pacific. This suggests that thermostad water upwelling in the eastern Pacific is one route by which the Pacific–Indian interbasin exchange is achieved.

*Acknowledgments.* This work was performed while BMS held a National Research Council Research Associateship Award at NOAA's Pacific Marine Environmental Laboratory (PMEL). Support was also provided through the NOAA Office of Global Programs (PAN American studies program) and the NOAA Office of Oceanic and Atmospheric Research. Timely comments from Peter Niiler on the effects of TIW on the equatorial heat budget were useful. Comments from two anonymous reviewers and Eric Firing improved the manuscript.

## REFERENCES

Anderson, D. L. T., and D. W. Moore, 1979: Cross-equatorial inertial jets with special relevance to very remote forcing of the Somali Current. *Deep-Sea Res.,* **26,** 1–26.

Barnier, B., L. Siefridt, and P. Marchesiello, 1995: Thermal forcing for a global ocean circulation model using a three year climatology of ECMWF analysis. *J. Mar. Sys.,* **6,** 363–380.

Baturin, N. G., and P. P. Niiler, 1997: Effects of instability waves in the mixed layer of the equatorial Pacific. *J. Geophys. Res.,* **102,** 27 771–27 793.

Bingham, F. M., and R. Lukas, 1995: The distribution of intermediate water in the western equatorial Pacific during January–February 1986. *Deep-Sea Res.,* **42,** 1545–1573.

Blanke, B., and S. Raynaud, 1997: Kinematics of the Pacific equatorial undercurrent: An Eulerian and Lagrangian approach from GCM results. *J. Phys. Oceanogr.,* **27,** 1038–1053.

Bryden, H. L., and E. C. Brady, 1985: Diagnostic model of the three-dimensional circulation in the upper equatorial Pacific Ocean. *J. Phys. Oceanogr.,* **15,** 1255–1273.

Butt, J., and E. Lindstrom, 1994: Currents off the east coast of New Ireland, Papua New Guinea, and their relevance to the regional undercurrents in the western equatorial Pacific Ocean. *J. Geophys. Res.,* **99,** 12 503–12 514.

Chelton, D. B., R. A. DeSzoeke, M. G. Schlax, K. El Naggar, and N. Siwertz, 1998: Geographical variability of the first baroclinic rossby radius of deformation. *J. Phys. Oceanogr.,* **28,** 433–460.

Church, J. A., and F. M. Boland, 1983: A permanent undercurrent adjacent to the Great Barrier Reef. *J. Phys. Oceanogr.,* **13,** 1747–1749.

Cromwell, T., 1953: Circulation in a meridional plane in the central equatorial Pacific. *J. Mar. Res.,* **12,** 196–213.

da Silva, A. M., C. C. Young, and S. Levitus, 1994: *Algorithms and Procedures.* Vol. 1, *Atlas of Surface Marine Data 1994,* NOAA Atlas NESDIS, 83 pp.

Delcroix, T., and C. Héin, 1988: Observations of the equatorial intermediate current in the western Pacific Ocean (165°E). *J. Phys. Oceanogr.,* **18,** 363–366.

——, G. Eldin, and C. Héin, 1987: Upper ocean water masses and transports in the western tropical Pacific (165°E). *J. Phys. Oceanogr.,* **17,** 2248–2262.

Fine, R. A., R. Lukas, F. M. Bingham, M. J. Warner, and R. H. Gammon, 1994: The western equatorial Pacific: A water mass crossroads. *J. Geophys. Res.,* **99,** 25 063–25 080.

Flagg, C. N., R. L. Gordon, and S. McDowell, 1986: Hydrographic and current observations on the continental slope and shelf of the western equatorial Atlantic. *J. Phys. Oceanogr.,* **16,** 1412–1429.

Gill, A. E., 1982: *Atmosphere–Ocean Dynamics.* Academic Press, 662 pp.

Gordon, A. L., R. D. Susanto, and A. Ffield, 1999: Throughflow within Makassar Strait. *Geophys. Res. Lett.,* **26,** 3325–3328.

Gouriou, Y., and T. Toole, 1993: Mean circulation of the upper layers of the western equatorial Pacific Ocean. *J. Geophys. Res.,* **98,** 22 495–22 520.

Gu, D., and S. G. H. Philander, 1997: Interdecadal climate fluctuations that depend on exchange between the tropics and extratropics. *Science,* **275,** 805–807.

Hansen, D. V., and C. A. Paul, 1984: Genesis and effects of long waves in the equatorial Pacific. *J. Geophys. Res.,* **89,** 10 431–10 440.

Hayes, S. P., J. M. Toole, and L. J. Mangum, 1983: Water-mass and

transport variability at 110° in the equatorial Pacific. *J. Phys. Oceanogr.,* **13,** 153–168.
Johnson, G. C., 2001: The Pacific Ocean subtropical cell surface limb. *Geophys. Res. Lett.,* **28,** 1771–1774.
——, and M. J. McPhaden, 1999: Interior pycnocline flow from the subtropical to the equatorial Pacific Ocean. *J. Phys. Oceanogr.,* **29,** 3073–3089.
——, ——, and E. Firing, 2001: Equatorial Pacific Ocean horizontal velocity, divergence, and upwelling. *J. Phys. Oceanogr.,* **31,** 839–849.
——, B. M. Sloyan, W. S. Kessler, and K. E. McTaggart, 2002: Direct measurements of upper ocean currents and water properties across the tropical Pacific during the 1990s. *Progress in Oceanography,* Vol. 52, Pergamon, 31–61.
Josey, S. A., E. C. Kent, and P. K. Taylor, 1999: New insights into the ocean heat budget closure problem from analysis of the SOC air–sea flux climatology. *J. Climate,* **12,** 2856–2880.
Kessler, W. S., 2002: Mean three-dimensional circulation in the northeast tropical Pacific. *J. Phys. Oceanogr.,* **32,** 2457–2471.
——, and B. A. Taft, 1987: Dynamic heights and zonal geostrophic transports in the central tropical Pacific during 1979–84. *J. Phys. Oceanogr.,* **17,** 97–122.
——, L. M. Rothstein, and D. Chen, 1998: The annual cycle of SST in the eastern tropical Pacific, as diagnosed in an ocean GCM. *J. Climate,* **11,** 777–799.
Kleeman, R., J. P. McCreary Jr., and B. A. Klinger, 1999: A mechanism for generating ENSO decadal variability. *Geophys. Res. Lett.,* **26,** 1743–1746.
Knauss, J. A., 1966: Further measurements and observations on the Cromwell Current. *J. Mar. Res.,* **24,** 205–240.
Lagerloef, G. S. E., G. T. Mitchum, R. G. Lukas, and P. P. Niiler, 1999: Tropical Pacific near-surface currents estimated from altimeter, wind, and drifter data. *J. Geophys. Res.,* **104,** 23 313–23 326.
Leetmaa, A., 1982: Observations of near-equatorial flows in the eastern Pacific. *J. Mar. Res.,* **40** (Suppl.), 357–370.
Lu, P., and J. P. McCreary Jr., 1995: Influence of the ITCZ on the flow of thermocline water from the subtropical to equatorial Pacific Ocean. *J. Phys. Oceanogr.,* **25,** 3076–3088.
——, ——, and B. A. Klinger, 1998: Meridional circulation cells and the source waters of the Pacific equatorial undercurrent. *J. Phys. Oceanogr.,* **28,** 62–84.
Lukas, R., 1986: The termination of the equatorial undercurrent in the eastern Pacific. *Progress in Oceanography,* Vol. 16, Pergamon, 63–90.
——, and E. Firing, 1984: The geostrophic balance of the Pacific equatorial undercurrent. *Deep-Sea Res.,* **31,** 61–66.
Macdonald, A. M., 1998: The global ocean circulation: A hydrographic estimate and regional analysis. *Progress in Oceanography,* Vol. 41, Pergamon, 281–382.
Meinen, C. S., M. J. McPhaden, and G. C. Johnson, 2001: Vertical velocities and transports in the equatorial Pacific during 1993–99. *J. Phys. Oceanogr.,* **31,** 3230–3248.
Moore, D. W., and S. G. H. Philander, 1977: Modeling the equatorial oceanic circulation. *The Sea,* E. D. Goldberg, Ed., Marine Modeling, Vol. 6, Wiley and Sons, 319–361.
Pedlosky, J., 1987: An inertial theory of the equatorial undercurrent. *J. Phys. Oceanogr.,* **17,** 1978–1985.
——, 1988: Entrainment and the termination of the equatorial undercurrent. *J. Phys. Oceanogr.,* **18,** 880–886.
——, 1991: The link between the western boundary currents and equatorial undercurrents. *J. Phys. Oceanogr.,* **21,** 1553–1558.
Picaut, J., and R. Tournier, 1991: Monitoring the 1979–1985 equatorial Pacific current transports with expendable bathythermograph data. *J. Geophys. Res.,* **96,** 3263–3277.
Poulain, P.-M., 1993: Estimates of horizontal divergences and vertical velocity in the equatorial Pacific. *J. Phys. Oceanogr.,* **23,** 601–607.
Rowe, G., E. Firing, and G. Johnson, 2000: Pacific equatorial subsurface countercurrent velocity, transport, and potential vorticity. *J. Phys. Oceanogr.,* **30,** 1172–1187.
Sloyan, B. M., and S. R. Rintoul, 2000: Estimates of area-averaged diapycnal fluxes from basin-scale budgets. *J. Phys. Oceanogr.,* **30,** 2320–2341.
——, and ——, 2001: Circulation, renewal and modification of Antarctic mode and intermediate water. *J. Phys. Oceanogr.,* **31,** 1005–1030.
Speer, K., and E. Tziperman, 1992: Rates of water mass formation in the North Atlantic Ocean. *J. Phys. Oceanogr.,* **22,** 93–104.
Tsuchiya, M., 1991: Flow path of Antarctic Intermediate Water in the western equatorial South Pacific Ocean. *Deep-Sea Res.,* **38,** s273–s279.
——, R. Lukas, R. A. Fine, E. Firing, and E. Lindstrom, 1989: Source waters of the Pacific equatorial undercurrent. *Progress in Oceanography,* Vol. 23, Pergamon, 101–147.
Weisberg, R. H., and L. Qiao, 2000: Equatorial upwelling in the central Pacific estimated from moored velocity profilers. *J. Phys. Oceanogr.,* **30,** 105–124.
Wunsch, C., 1996: *The Ocean Circulation Inverse Problem.* Cambridge University Press, 442 pp.
Wyrtki, K., 1981: An estimate of equatorial upwelling in the Pacific. *J. Phys. Oceanogr.,* **11,** 1205–1214.
——, and B. Kilonsky, 1984: Mean water and current structure during the Hawaii-to-Tahiti Shuttle experiment. *J. Phys. Oceanogr.,* **14,** 242–254.